Assessment of integrated energy systems for the production and use of renewable methanol by water electrolysis and CO_2 hydrogenation

Francesco Lonis [a*], Vittorio Tola [a,1)], Giorgio Cau [a,2)]
a) Department of Mechanical, Chemical and Materials Engineering, University of Cagliari, Via Marengo 2, 09123 Cagliari, Italy
* francesco.lonis@unica.it +39 070 675 5741
1) vittorio.tola@dimcm.unica.it
2) gcau@unica.it

Abstract

The conversion of renewable hydrogen and recycled CO_2 to valuable fuels in power-to-liquids (PtL) systems could be a key solution to reduce CO_2 emissions. Within this context, methanol is a promising candidate, both as an energy carrier and a chemical feedstock.

This paper is focused on renewable methanol production and its use in a PtL integrated system based on a water electrolysis process fed by RES, a methanol synthesis and purification section and a high temperature solid oxide fuel cell. In particular, an analysis and comparison of two power-to-methanol integrated systems based on different electrolysis technology, i.e. the commercially mature alkaline electrolysers and the innovative high temperature solid oxide cells, was carried out. A thermal energy storage system based on a phase change material and an organic Rankine cycle engine can also be included, depending on the chosen electrolysis process.

Detailed models of the main sections were developed and implemented by using Aspen Plus. A comprehensive analysis through mass and energy balances was carried out to evaluate performance indices of each section and of the overall plant for the two different configurations. A global efficiency of the overall system slightly lower than 0.35 was obtained for both systems.

Keywords: alkaline electrolysis; solid oxide cells; methanol; CO_2 hydrogenation; energy storage; power-to-liquids

Acronyms

AEL	Alkaline electrolyser/electrolysis	ORC	Organic Rankine cycle
BOP	Balance of plant	P	Pump
C	Cooler	PC	Post combustor
CP	Compressor	PCM	Phase change material
D	Distillation column	PtL; PtX	Power-to-liquids; Power-to-X
DME	Dimethyl ether	R	Reactor
F	Flash	RES	Renewable energy sources
FT	Fischer-Tropsch	RF	Reformer
H	Heater	RSOC	Reversible solid oxide cell
HX	Heat exchanger	S	Splitter
IC	Intercooler	SOC	Solid oxide cell
LHV	Lower heating value	SOEC	Solid oxide electrolyser cell
M	Mixer	SOFC	Solid oxide fuel cell
MeOH	Methanol	T	Turbine
MSS	Methanol synthesis section	TES	Thermal energy storage

Equation Symbols

$a_{H_2O,KOH}$	Water activity	η_{PtL}	Power-to-liquid efficiency
E_0	Reversible potential [V]	φ_{AEL}	SOEC-MSS corrective factor
E_{AEL}	Electrolyser net voltage (AEL) [V]	F	Faraday constant [C/mol]
$E_{act,an}$, $E_{act,cat}$	Activation energy levels [J/mol]	N_S	Number of cells in AEL stack
E_{eq}	Equilibrium voltage [V]	p	Cell operating pressure [bar]
$\dot{E}_{MSS}$	MSS inlet external power [kW]	$p_{v,KOH}$	Vapour pressure KOH solution
E_{SOEC}	Electrolyser net voltage (SOEC) [V]	p_i	Electrodes partial pressure [Pa]
E_{SOFC}	Cell net voltage (SOFC) [V]	P_{AEL}	AEL electric power [kW]
η_{act}	Activation overpotentials (SOEC) [V]	$P_{BOP,AEL}$	AEL auxiliaries power [kW]
η_{conc}	Concentration overpotentials (SOEC) [V]	$P_{BOP,MSS}$	MSS auxiliaries power [kW]
η_{ohm}	Ohmic overpotential (SOEC) [V]	P_{SOEC}	SOEC electric power [kW]
η_{ele}	Electrolysis efficiency	$P_{BOP,SOEC}$	SOEC auxiliaries power [kW]
n_F	Faraday efficiency	P_{SOFC}	SOFC electric power [kW]
η_G	System global efficiency	$P_{BOP,SOFC}$	SOFC auxiliaries power [kW]
$\eta_{ele,R}$	Rectified electrolysis efficiency	P_{ORC}	ORC electric power [kW]
η_{MSS}	MSS efficiency	$P_{BOP,ORC}$	ORC auxiliaries power [kW]
$\eta_{MSS,C}$	MSS chemical conversion efficiency	R	Universal gas constant [J/(mol K)]
η_{SOFC}	SOFC efficiency	r_{CH_3OH} , r_{CO}	Methanol and CO reaction rates
$\eta_{SOFC+ORC}$	SOFC efficiency with ORC	T_c	Cell operating temperature [K]
LHV_i	Lower heating value [kJ/kg]	V_{act}	Activation overpotentials (AEL) [V]
$\dot{m}_i$	Mass flow rate [kg/s] or [kg/h]	V_{ohm}	Ohmic overpotentials (AEL) [V]

1. Introduction

In the context of the energy transition challenge, power-to-X (PtX) technologies coupled to renewable energy sources (RES) and captured CO_2, might play a crucial role reducing CO_2 emissions and substituting products derived from fossil fuels [1,2]. Indeed, the "X" represents a wide variety of products, such as liquid and gaseous fuels (gasoline, kerosene, ethanol, methanol, methane, hydrogen, syngas, etc.), chemicals, and others, that could be employed in many different sectors, with net CO_2 emissions near to zero [3,4]. In addition, PtX systems can provide a variety of chemicals, services and commodities in several sectors [5–8]: production of hydrogen and hydrogen carriers [9]; fuels for power generation and combined heat and power [10]; heat production [11,12]; transportation [13–16]; energy storage and grid ancillary services as well as grid balancing [10,17,18]; production of chemical compounds and fuels (i.e. methanol, dimethyl ether DME, formaldehyde, gasoline, diesel fuel, methane, syngas etc.) [19–21]. PtX technologies can boost RES penetration and reliability, allowing the storage of excess renewable energy in long-term and high-energy density storage systems, while creating a closed carbon cycle with near zero net CO_2 emissions [22,23].

In this framework, numerous studies regarding power-to-X and power-to-liquids (PtL) systems based on different technologies and approaches can be found in literature, as for example, H_2 production and compression, production of mixed alcohols and other liquids through Fischer-Tropsch (FT), hydrogen to liquids, power and biomass to liquids, methanol production, etc.

Efficiency-wise, depending on the considered technology and pathway, conversion values of PtX spanning from 37 to 70% were found. In particular, Mignard and Pritchard [24] analysed different processes to synthesise liquid fuels exploiting renewable marine energy and CO_2 for the production of hydrogen at high pressure. Hydrogen is further converted into methanol, mixed alcohols through FT and gasoline using the Mobil process, obtaining efficiencies ranging from a minimum of 42% (gasoline via Mobil) to a maximum of 61% (compressed hydrogen at 400 bar). O'Brien et al. [25] simulated a process with a UniSim model to evaluate the performance of a large-scale (300 MW_e) high temperature co-electrolysis plant producing syngas and liquid fuels by FT, exploiting steam and CO_2. The overall process efficiency was assessed between 43 and 44%. Graves at al. [26] carried out a critical review of different

pathways for recycling CO_2 into useful fuels exploiting renewable or nuclear energy (both characterised by zero CO_2 emissions), based on CO_2 capture, H_2O and CO_2 dissociation, and fuel synthesis. The authors [26] analysed technologies such as thermolysis, thermo-chemical cycles, electrolysis and photo-electrolysis, as well as high temperature co-electrolysis of water and CO_2, CO_2 direct air capture using solid sorbents and conversion of syngas into fuels by FT processes. They found that an energy system based on direct air CO_2 capture, co-electrolysis of water and CO_2 in a solid oxide cell, and FT conversion to liquid fuels achieves an electricity-to-liquid fuel efficiency of approximately 70%. Crivellari et al. [27] analysed two innovative schemes to produce methanol from combined wind and solar power within an offshore oil & gas platform. One of the solutions is based on methanol production through CO_2 hydrogenation from renewables, water and external CO_2, while the other also exploits useful by-products of the oil & gas process. The authors [27] found that the synergy between the renewable methanol production and the oil & gas activities can counterbalance the footprint of such processes, also providing multiple valuable fuels. Albrecht et al. [28] analysed the opportunity of using PtL plants in energy storage applications, finding that a system composed of solid oxide cells and FT synthesis produces a mixture of gasoline, kerosene and diesel fuel with an efficiency of 37% and 44%, considering a single-way or a reversible systems, respectively. Furthermore, Albrecth et al. [29,30] carried out a comprehensive and detailed techno-economic evaluation of alternative and cleaner approaches to produce jet fuel and other liquid fuels. In particular, a biomass-to-liquids, a power- and biomass-to-liquids, and a PtL process were analyzed, showing an X-to-liquids efficiency of 36.3%, 51.4% and 50.6%, respectively. The corresponding overall plant efficiency achieved considering the by-products (i.e. electricity and the useful recoverable heat) were 82.6%, 65.0%, and 66.8%. Fasihi et al. [31] carried out a techno-economic assessment of a PtL process based on hybrid photovoltaic-wind power plants integrated with a FT process, finding an overall energy efficiency of 65% for a liquid fuel mixture composed of 15% naphtha, 25% jet fuel, and 60% diesel. Also, the authors [31] demonstrated the competitiveness of such systems compared to conventional fossil fuel diesel production. Schmidt et al. [13,32] proposed the PtL technology as a solution to produce green and

sustainable methanol and aviation fuel. Different approaches such as low and high temperature electrolysis, CO_2 capture from the atmosphere or from concentrated sources, methanol production or liquids fuel by FT, were considered. An efficiency of the methanol synthesis equal to 39% was obtained when coupled to direct CO_2 capture, improving to 48% in case of concentrated CO_2 capture [32]. For the aviation liquid fuels (LHV of 42 MJ/kg), the efficiency increases from 39% to 47%, switching from direct to concentrated CO_2 capture [13]. Michailos et al. [33] carried out in Aspen Plus a techno-economic assessment on a system to synthesise DME following a power-to-liquids concept. The authors [33] found an overall efficiency of 44.4% with a CO_2 conversion to DME of 82.3%.

From the economic point of view, the production of renewable fuels from RES and captured CO_2 will be more expensive than fossil fuel, but cheaper than biofuels [34]. Nevertheless, nowadays RES shows a levelised cost of energy of RES in the range of that of fossil fuels (0.050 to 0.170 USD/kWh), even without considering the RES incentives and the drawbacks caused by fossil fuels emissions, defining a promising future for these applications [35,36]. For example, in Europe, RES costs have dropped between 0.08 (onshore wind power) and 0.15 (offshore wind power) USD/kWh [35]. Indeed, the highest cost in PtX processes based on renewable hydrogen production and use is related to the electrolysis process (covering roughly 80% of the total energy costs of PtX systems). Nevertheless, in future perspective, these costs are expected to drop sensibly, allowing the PtX technologies to become advantageous compared to conventional fuel production, also considering future restrictions and taxation on CO_2 emissions [37–40].

Among the PtX technologies, power-to-methanol is of particular importance thanks to the potential use of this chemical compound. Indeed, methanol is widely recognised as a fuel with many different uses as an energy feedstock, a hydrogen carrier and as a chemical compound [41–43]. At ambient conditions, methanol is a liquid characterised by a high energy density by volume compared to hydrogen, so resulting a good energy storage medium, not being affected by long-term decomposition or energy losses. A variety of chemical compounds, typically derived from fossil fuels, can be produced using methanol as a chemical feedstock:

formaldehyde, DME, acetic acid, gasoline, diesel and many others [2], leading to the prospect of a future methanol economy [4,43,44].

Worldwide, the only existing power-to-methanol commercial-scale plant is located in Iceland (George Olah Plant [45]). The plant produces approximately 4000 $\mathrm{t/year}$ of methanol with an electrical power requirement of 6 MW, assuring a consumption of 5500 $\mathrm{t/year}$ of captured CO_2 [46,47]. In the plant the production of a 1 t of methanol requires 0.19 t of hydrogen obtained through an alkaline water electrolysis process fed by RES and 1.38 t of CO_2 recovered from the geothermal plant located nearby. Since the hydrogen is produced from RES, the methanol production reduces the life-cycle carbon footprint by about 90-99% compared to gasoline or diesel fuel. Even compared to the methanol production from natural gas, renewable methanol allows a reduction of the overall CO_2 emissions by 1.53 t per t of produced methanol [47]. Even though precise data are not available about the Olah plant overall efficiency, Bergins et al. [48] estimated an efficiency of approximately 61% for a power-to-methanol plant with a capacity production of about 400 $\mathrm{t/day}$ based on RES (50-150 MW_e electrolysers) and post combustion CO_2 capture from a conventional coal power plant.

This paper is within the context of a research project on power to-methanol systems carried out by the same authors. In a previous paper [49] a power-to-methanol system based on a reversible solid oxide cell (RSOC) [50,51], integrated with a thermal energy storage (TES) system was studied. The overall system was characterized by a global efficiency of about 0.33. In this paper, the thermal integration in each section was optimised. Moreover, the less conventional system based on RSOC was compared with a more commercial mature system based on a AEL In addition, a smaller plant was considered to align the power produced in SOFC operation to the state of the art of commercial modules, characterised by a maximum power output of 1 MW.

This work is focused on the analysis and comparison of two power-to-methanol integrated systems based on different electrolysis technology, i.e. alkaline electrolysers (AEL) and high temperature solid oxide cells (SOEC) [52,53], to perform renewable energy storage. Renewable hydrogen produced exploiting excess RES reacts with captured CO_2 producing methanol in a

synthesis reactor. Methanol is purified and then stored (charge phase of the energy storage system). Then, methanol feed the SOFC producing electricity when necessary. Depending on the chosen configuration, waste heat contained in the exhaust gases of the SOFC is either stored in a TES system to reduce the thermal requirements in electrolysis operation or used in an organic Rankine cycle (ORC) to boost the electricity production of the plant during the discharge phase. In case of SOEC configuration, the system was supposed to be based on a RSOC, capable of operating alternatively as an SOEC to produce hydrogen and as an SOFC to produce electricity, reducing the plant components. RSOCs are developed from the affirmed SOFC technology and operate typically in a temperature range between 700 and 1000 °C in both fuel cell and electrolyser mode [54,55]. The high temperature operation guarantees high efficiencies in both modes thanks to better reaction kinetics and lower electrochemical losses.

Several performance indices were specifically defined to evaluate the efficiencies of each section and of the overall system through energy and mass balances. The simulations of the considered energy systems were carried out in Aspen Plus environment, where special models were developed to simulate the electrolysis and fuel cell processes, the methanol synthesis and purification processes, as well as the ORC engine. The two integrated systems and their subsystems were compared through the analysis of appropriate performance indices.

2. Overall system configuration

The general configuration of the overall system includes a water electrolysis section, a methanol synthesis section (MSS), a SOFC, an ORC engine system, a thermal energy storage (TES) system and a heat integration section comprising heaters to boot the system. As previously specified, the water electrolysis is performed considering the commercially mature technology of alkaline electrolysers (case A) or the innovative technology of solid oxide electrolysers (case B). The ORC and the TES sections are optional, depending on the case. The system operates in charge phase when electricity in excess is stored as chemical power into methanol, and in discharge phase when the stored methanol is used to produce electricity. Fig. 1 shows a simplified functional scheme of the general configuration of the overall system.

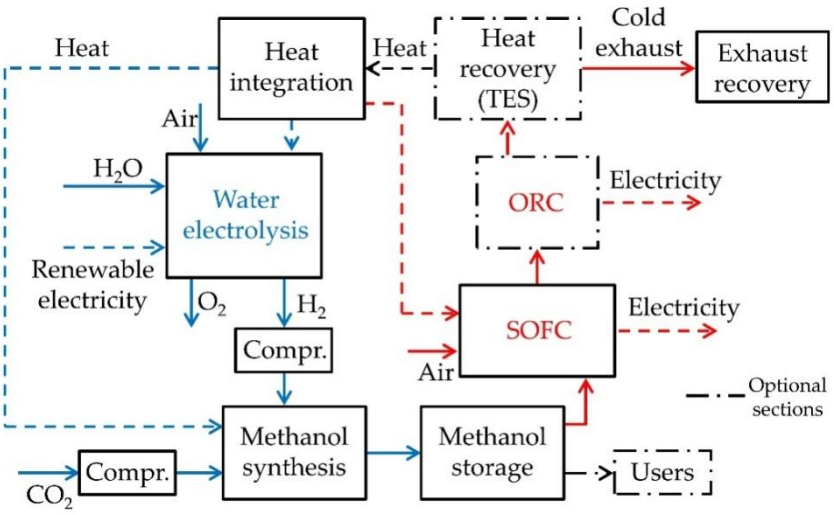

Fig. 1 – Simplified functional scheme of the overall system

Water and renewable electricity feed the electrolyser to produce hydrogen. Hydrogen and CO_2 are compressed at the operating pressure of the methanol synthesis reactor in two intercooled compressor trains. In the MSS, CO_2 hydrogenation to methanol is carried out over a commercial catalyst ($Cu/ZnO/Al_2O_3$) and methanol is separated and purified in a distillation column. During the discharge phase, methanol is reformed and oxidised in a solid oxide fuel cell to produce electricity, while exhaust gases, rich in H_2 and CO, are burnt in a post-combustor. The heat released during SOFC operation is either supplied to an ORC engine (case A) or stored in a TES system (case B) to provide thermal energy to the SOEC process. The “Users” block represents another opportunity for this kind of systems, where the produced methanol can be used in different applications than energy storage for electricity production, as for example as a feedstock in chemical industry or as a fuel in other applications.

RSOC systems, typically derived from SOFC, are characterised by a maximum power of 30-50 kW when operated as SOFC and a power requirement of about 150 kW when operated as SOEC [56]. Nevertheless, SOFCs are available with a maximum power of 1 MW [57]. For the sake of comparison, the overall systems were both sized to produce 1 MW of electric power with the SOFC, assuming that RSOCs will be scaled up to SOFC typical power in the future. The flow rates of the streams of all the sections were calculated with reference to such a SOFC power.

3. Modelling of the main sections of the overall system

3.1. System based on alkaline water electrolysis

Firstly, the configuration based on more commercial mature technologies was studied (case A). In particular, the overall system is composed of:

- An alkaline water electrolyser,
- A methanol synthesis and purification section,
- A solid oxide fuel cell,
- An organic Rankine cycle device.

Since the AEL operates at low temperature, the heat released during SOFC operation might be used or stored for different applications, such as the introduction of an ORC or to produce hot district water. The ORC is in series with the SOFC, it is fed with the hot exhaust gases of the latter and it allows an enhanced production of electricity, increasing the overall system efficiency. As previously specified, the size and characteristics of the AEL-based system were all defined with reference to the SOFC nominal power of 1 MW_e.

3.1.1. Alkaline water electrolyser

Alkaline electrolysis of water is a low temperature process to produce hydrogen in a commercially mature technology, namely the alkaline electrolyser. Water electrolysis is carried out in a liquid alkaline electrolyte solution of a base (KOH or $NaOH$), where hydroxide ions OH^- cross a diaphragm separating the electrodes. Typically, AELs operate between 60 and 90 °C, while the operating pressure spans from ambient pressure up to 35 bar [58]. In this work the alkaline water electrolysis is performed at 25 bar and 65 °C, leading to a specific energy consumption of approximately 45 kWh/kg_{H_2} (4.01 $kWh/Nm^3_{H_2}$), consistent with values reported in the literature [59,60].

An existing electrochemical model for the simulation of a commercial AEL, originally developed by Ursua and Sanchis [59], was implemented in the Fortran routines of Aspen Plus. To make the system scalable, depending on the desired hydrogen production and on the voltage and current values, different arrangement in series and parallel can be chosen. Since the molar water flow rate is the same as that of hydrogen for each cell, it can be calculated from Eq. (1):

$$n_{H_2} = \frac{I}{2\,F} \quad (1)$$

where n_{H_2} are the moles of produced hydrogen, I is the electric current and F is the Faraday's constant. Considering a nominal current of 120 A as in Ursúa and Sanchis [59], a production of approximately $6.22 \cdot 10^{-4}$ $\mathrm{mol_{H_2}}/s/\mathrm{cell}$ was achieved. Given the desired hydrogen flow rate, the total number of cells was calculated.

Since the electrolyser is characterised by parasitic current loss, a Faraday efficiency η_{F}, defined as the ratio between the actual hydrogen production rate and the theoretical production, was considered. This efficiency is bound to the characteristic of the electrolyser and depends on the operating temperature. In this study the Faraday efficiency empirical relation developed by Ulleberg [61] and reported by Eq. (2), was applied:

$$\eta_F = a_1\, exp\left(\frac{a_2 + a_3 T_c + a_4 T_c^2}{I/A} + \frac{a_5 + a_6 T_c + a_7 T_c^2}{(I/A)^2}\right) \quad (2)$$

where $\mathrm{T_c}$ is the cell operating temperature and A is the active area of the cell. Table 1 reports the value of the other parameters used to calculate the Faraday efficiency as Eq. (2).

Table 1 – Parameters for the Faraday efficiency calculation [61]

a_1	a_2 $[\mathrm{m^2A^{-1}}]$	a_3 $[\mathrm{m^2A^{-1}{\circ}C^{-1}}]$	a_4	a_5 $[\mathrm{m^2A^{-1}}]$	a_6 $[\mathrm{m^2A^{-1}{\circ}C^{-1}}]$	a_7
0.995	-9.5788	-0.0555	0	1502.7083	-70.8005	0

A simplified functional scheme of the model of the AEL as it was implemented in Aspen Plus is reported in Fig. 2.

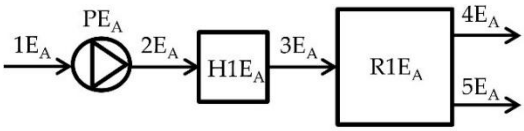

Fig. 2 – Simplified functional scheme of the alkaline electrolyser section

In Fig. 2, water ($1E_A$) is pumped (PE_A) and heated up ($H1E_A$) to the cell operating temperature before feeding the reactor ($R1E_A$). Since the operating voltage of one cell (1.70 V at 65 °C and 25 bar) is above the thermoneutral voltage at the same conditions (1.47 V), due to the low temperature operation, the heat produced by the Joule effect can be used to preheat the inlet

water. Inside $R1E_A$ the water splitting reactions are carried out producing hydrogen ($3E_A$) and oxygen ($4E_A$). The reactor was modelled as a stoichiometric reactor (RStoic block in the Aspen Plus environmental). Since the utilisation factor is set to 1 a water flow rate of approximately 675 kg/h is necessary to produce the 76 kg/h hydrogen stream required by the MSS to obtain the desired methanol production.

The electrochemical behaviour and the characteristic curves of the electrolyser are defined by the comprehensive model implemented in a Fortran routine. The equilibrium voltage of the stack is expressed as a function of temperature and pressure according to Eq. (3):

$$E_{eq} = N_S \left[E_0 + \frac{RT_c}{2F} ln \left(\frac{(p - p_{v,KOH})(p - p_{v,KOH})^{\frac{1}{2}}}{a_{H_2O,KOH}} \right) \right] \quad (3)$$

where the term N_S indicates the number of cells of a stack, E_0 is the reversible potential of one cell; p and $p_{v,KOH}$ are the stack operating pressure and the vapour pressure of the KOH solution, while $a_{H_2O,KOH}$ represents the water activity in the KOH solution.

The reversible potential E_0 is calculated by means of Eq. (4):

$$E_0 = 1.5184 - 1.5421 \times 10^{-3}\, T_c + 9.526 \times 10^{-5}\, T_c\ ln(T_c) + 9.84 \times 10^{-8}\, T_c^2 \quad (4)$$

Finally, the AEL net voltage E_{AEL} is evaluated adding to the equilibrium potential E_{eq} the overvoltages caused by the ohmic and activation resistances as shown in Eq. (5):

$$E_{AEL} = E_{eq} + \left[V_{ohm} + V_{act,an} + V_{act,cat} \right] \quad (5)$$

The electrochemical model developed in Aspen Plus was validated through a comparison with the experimental results reported by Ursúa and Sanchis [59]. The validation was carried out at 25 bar for temperature values of 15, 35 and 65 °C (as the experimental tests in [59]). Table 2 reports the values of the main parameters considered for the validation.

Table 2 – Parameters used in AEL model validation

Parameter	Value
Temperature [°C]	15, 35, 65 °C
Operating pressure [bar]	25

Number of cells	22
Cell area [cm^2]	300

Figure 3 shows the comparison between the results of the model developed in Aspen Plus and the experimental ones reported by Ursúa and Sanchis.

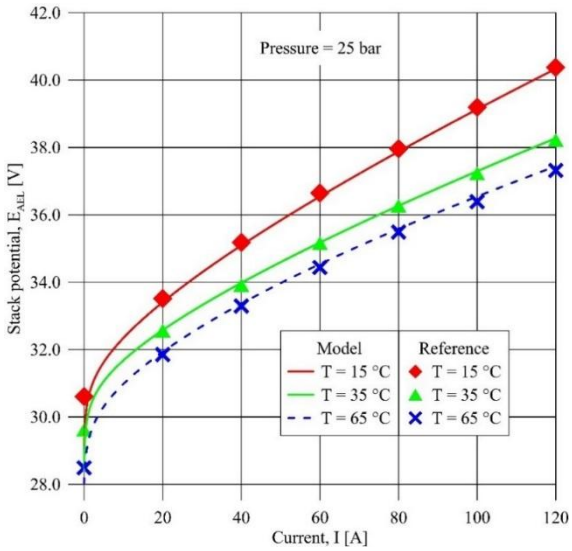

Fig. 3 – Comparison between numerical results and experimental data (AEL)

As can be seen from Fig. 3, the Aspen Plus model follows the reference experimental curves closely, leading to an accurate evaluation of the system voltage and, consequently, of its power consumption and efficiency.

Figure 4 represents the power consumption (left) and efficiency (right) of the AEL as a function of the pressure, for different temperatures of the cell, whereas Fig. 5 represents the same performance characteristics as a function of temperature, for different pressures of the cell.

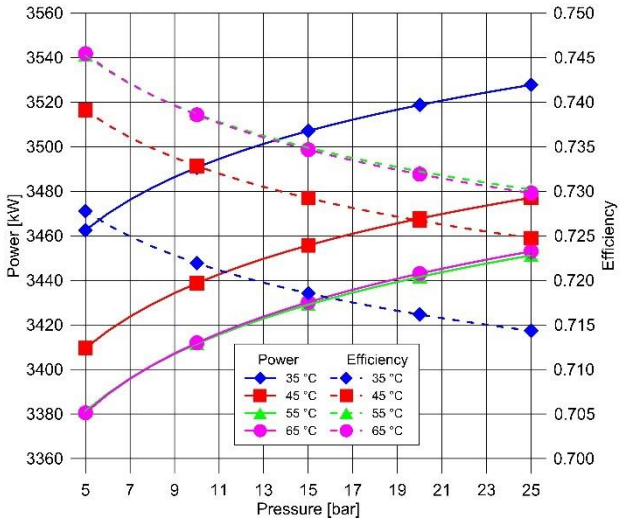

Fig. 4 – Power-pressure (left) and efficiency-pressure (right) characteristics

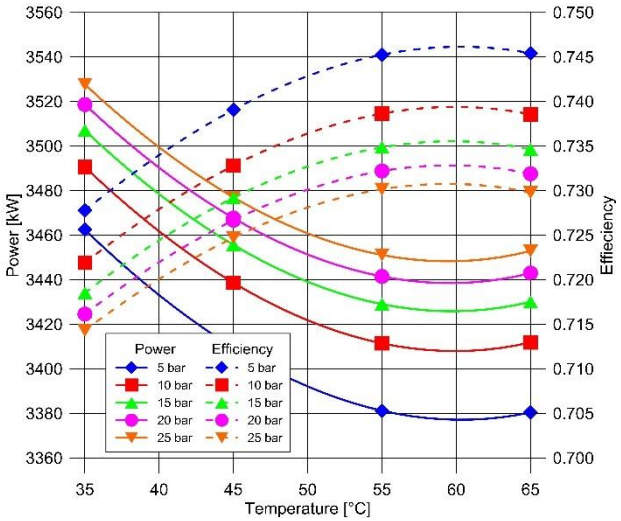

Fig. 5 – Power-temperature (left) and efficiency-temperature (right) characteristics

For a given cell temperature, an increase of the cell pressure leads to a greater power consumption and to an efficiency reduction. On the contrary, for a given cell pressure, an increase of the temperature reduces the power consumption and boosts the efficiency.

Even though a higher electrolysis pressure causes an increase in the consumed power in the AEL, a higher pressure reduces the power required by the hydrogen compressors in the methanol synthesis section. Assuming AEL operating pressures of 5 and 25 bar, the power absorbed by the AEL is equal to 3381 kW and 3453 kW, respectively,

3.1.2. Methanol synthesis section

Downstream of the electrolyser, the methanol synthesis section allows the production of the liquid fuel used to store energy. The main blocks in the MSS are: the adiabatic reactor, where the catalytic CO_2 hydrogenation process is carried out, and the distillation column, where the purification process is carried out [62]. Methanol is produced through the three main reactions of the CO_2 hydrogenation process: CO is given by the water gas shift reaction (6) and converted into methanol by the CO hydrogenation reaction (7), while methanol is also produced through the CO_2 hydrogenation reaction (8).

$$CO_2 + H_2 \rightleftarrows CO + H_2O \quad (6)$$

$$CO + 2H_2 \rightleftarrows CH_3OH \quad (7)$$

$$CO_2 + 3H_2 \rightleftarrows CH_3OH + H_2O \quad (8)$$

The catalytic reaction was simulated through an LHHW kinetic model especially developed in Aspen Plus [62,63]. A detailed description of the process and of the kinetic model used is reported in Lonis et al. [49].

In this study all the methanol produced in the MSS is used in the SOFC. For the sake of simplicity, the charging and discharging processes are considered of the same duration.

The production and consumption of methanol were set considering the power of 1 MW. This corresponds to 76 kg/h of hydrogen and 550 kg/h of CO_2 (equal to about 840 and 280 Nm^3/h, respectively), from which 370 kg/h of methanol are produced.

The compression of the reactants is carried out through The methanol synthesis reactor operates at 65 bar requiring the hydrogen and CO_2 to be compressed. While the CO_2 compressor train is composed of three compressors characterised by an intercooling temperature of 38 °C and a compression ratio of about 4, the number of compressors for the H_2 depends on the operating electrolysis pressure. In particular, three different configurations were analysed for the alkaline electrolyser: a) AEL operating pressure of 5 bar and two intercooled compressors in the MSS, b) AEL operating pressure of 5 bar and three intercooled compressors in the MSS, and c) AEL operating pressure of 25 bar and one compressor in the MSS. Table 3 summarises the power requirements of the compressors for the different configurations.

Table 3 – Methanol synthesis: hydrogen compression power

AEL pressure	1st compr. [kW]	2nd compr. [kW]	3rd compr. [kW]	Total [kW]
5 bar (2 compr.)	53.6	63.6	/	117.2
5 bar (3 compr.)	33.5	38.5	38.9	110.9
25 bar (1 compr.)	37.9	/	/	37.9

The configuration with one compressor allows saving about 70 kW in comparison to that with multiple compressors. This value compensates for the larger AEL power absorption in case of 25 bar operation (72.5 kW, as shown in Fig. 4). Hence, to reduce the complexity of the system,

25-bar was chosen as operating pressure of the AEL, allowing the use of only one compressor in the MSS. Since the compression power required by the CO_2 is equal to 56 kW the total power absorbed by the compressors in the MSS is about 94 kW.

The MSS simplified functional scheme is presented in Fig. 6.

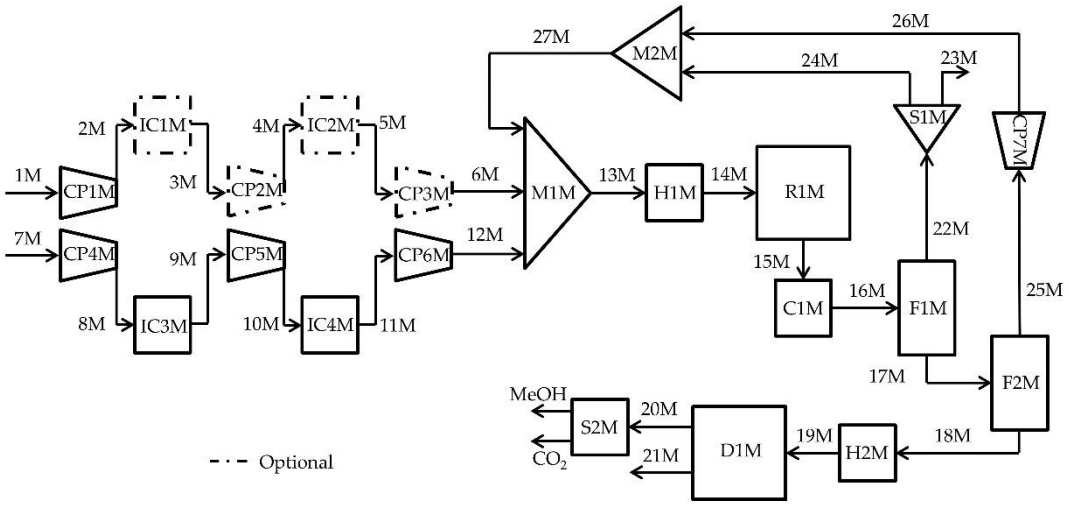

Fig. 6 – Simplified functional scheme of the methanol synthesis and purification section (C = Cooler; CP = Compressor; D = Distillation column; F = Flash; H = Heater; IC = Intercooler; M = Mixer; R = Reactor; S = Splitter)

The compressed H_2 (6M) and CO_2 (12M) are mixed with the re-circulated gases (27M) and preheated (H1M) to 210 °C prior to entering the synthesis reactor (R1M). Within the adiabatic reactor, the exothermal CO_2 hydrogenation reaction increases the temperature up to 290 °C. The reactor outlet is mainly composed of hydrogen (about 77% by vol.), whereas the methanol content is lower than 4% by volume (Table 4). To boost the production of methanol, two flash processes are performed (F1M and F2M) and the un-reacted incondensable gases (22M and 25M) are re-circulated back to the reactor. The first flash occurs at 65 bar, after reducing the temperature to 50 °C in a cooler (C1M). The second flash process takes place reducing the pressure and temperature of the liquid stream to about 1.2 bar and 22 °C. The resulting liquid product (18M), namely crude methanol, is mainly composed of methanol and water (both about 49% by vol.) with a small content of CO_2. To boost the methanol purity, the separation of water and methanol takes place in a distillation column (D1M). The distillate at the top of the column (20M) is a mixture of methanol and CO_2, with a methanol purity of 96.4% (by volume). Subsequently methanol and CO_2 are easily separated by condensing the former.

345 Tables 4a and 4b summarise the main parameters (i.e. mass flow, temperature, and molar
346 fraction) of the main streams in the MSS.

Table 4a – Mass flow, temperature and composition (by volume) of the main streams in the MSS

	1M/2M	3M/4M	5M/6M	7M/8M	9M/10M	11M/12M	13M/14M	15M/16M
Mass flow [kg/s]	0.021	0.021	0.021	0.153	0.153	0.153	0.860	0.860
Temp [°C]	25/219	38/240	38/240	25/159	38/176	38/179	75/210	291/50
CH_3OH	0.0000	0.0000	0.0000	0.0000	0.0000	0.0000	0.0031	0.0384
H_2O	0.0000	0.0000	0.0000	0.0000	0.0000	0.0000	0.0012	0.0369
CO_2	0.0000	0.0000	0.0000	1.0000	1.0000	1.0000	0.1297	0.1032
H_2	1.0000	1.0000	1.0000	0.0000	0.0000	0.0000	0.8210	0.7729
CO	0.0000	0.0000	0.0000	0.0000	0.0000	0.0000	0.0450	0.0486

347

Table 4b – Mass flow, temperature and composition (by volume) of the main streams in the MSS

	17M	18M/19M	20M	21M	22M	24M	25M/26M	27M
Mass flow [kg/s]	0.214	0.167	0.109	0.059	0.646	0.639	0.047	0.686
Temp [°C]	50	22/80	63	100	50	50	22/485	57
CH_3OH	0.4260	0.4874	0.9640	0.0000	0.0030	0.0030	0.0535	0.0036
H_2O	0.4259	0.4944	0.0000	1.0000	0.0013	0.0013	0.0098	0.0014
CO_2	0.1459	0.0182	0.0360	0.0000	0.0993	0.0993	0.9209	0.1099
H_2	0.0000	0.0000	0.0000	0.0000	0.8435	0.8435	0.0003	0.8327
CO	0.0022	0.0000	0.0000	0.0000	0.0529	0.0529	0.0155	0.0524

348

349 Since the reactor products are characterized by a high temperature (about 290 °C), they can be
350 employed to provide heat to some processes within the MSS, reducing the thermal energy that
351 otherwise would be provided by an external source. In particular, thermal energy is required by
352 the following MSS processes:

353 - the preheating of the reactants (13M) from 75 to 210 °C,
354 - the distillation process (occurring at 100 °C),

- the heating of crude methanol up to the inlet temperature of the distillation column (80 °C).

Figure 7 shows the simplified functional scheme of the methanol synthesis section taking into account the thermal integrations within the section.

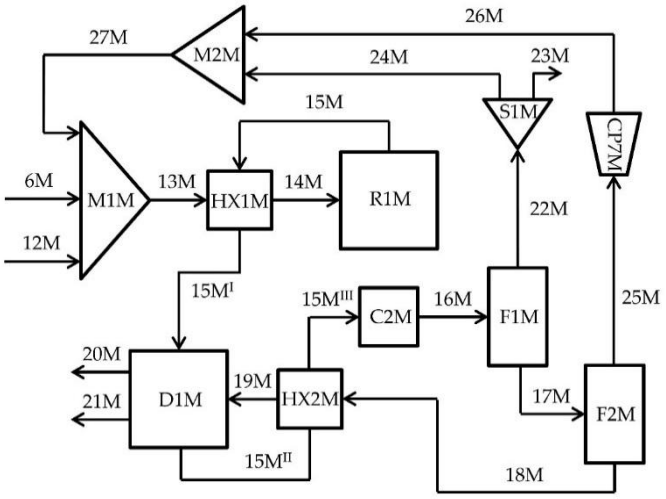

Fig. 7 – Simplified functional scheme of the methanol synthesis and purification section with thermal integrations (C = Cooler; CP = Compressor; D = Distillation column; F = Flash; HX = Heat exchanger; M = Mixer; R = Reactor; S = Splitter)

Firstly, the reactor products are cooled from from 290 (15M) to 175 °C ($15M^{I}$) realising about 350 kW to the reactants (HX1M). Then, the reactor products release 180 KW in the distillation column (D1M), reducing their temperature to 124 °C). Finally, the reactor products are cooled to about 105 °C (HX2M) with the preheating of the crude methanol ($15M^{II}$) and allowing a recovery of roughly 135 kW. To reach the first flash condition (50 °C), roughly 235 kW should be further removed from the reactor products in the cooler C2M. Globally, a total power of approximately 665 kW is recovered and exploited within the MSS, reaching the thermal self-sustainability of the section. In Table 5 the heating and cooling processes within the MSS are summarised.

Table 5 – Main heat transfers in the MSS

Heating process	Heat [kW]	Cooling process	Heat [kW]
Reactor inlet by heat recovery (HX1M)	350.3	Reactor outlet 1st cooling (HX1M)	-350.3
Distillation reboiling by heat recovery (D1M)	180.0	Reactor outlet 2nd cooling (D1M)	-180.0
Crude methanol by heat recovery (HX2M)	135.2	Reactor outlet 3rd cooling (HX2M)	-135.2
		Reactor outlet 4th cooling (C2M)	-233.7

3.1.3. Solid oxide fuel cells

Solid oxide fuel cells typically operate in a temperature range between 700 and 1000 °C. The high temperature operation guarantees high efficiencies thanks to better reaction kinetics and lower electrochemical losses. In addition, being composed of ceramic materials and metal alloys, SOFC are not subjected to deactivation and CO poisoning and can operate with a variety of fuels, with different grades of purity.

Solid oxide fuel cells produce electricity following reactions (9) and (10):

$$2H_2 + 2O^{2-} \rightarrow 2H_2O + 4e^- \quad (9)$$

$$2O_2 + 4e^- \rightarrow 2O^{2-} \quad (10)$$

To simulate the operation of the SOFC an electrochemical model derived from Ni et al. [64] was implemented within the Aspen Plus environment. Three main equations were considered to simulate the SOFC. A comprehensive description of the adopted model and used parameters can be found in Lonis et al. [49].

The SOFC is fed by methanol that is reformed inside the fuel cell along with water to produce the hydrogen required for the SOFC reactions. The SOFC is also fed by air to provide the required oxygen. To guarantee the design power production of 1 MW, a methanol flow rate of 370 kg/h is required, corresponding to the methanol production in the MSS, since the duration of the charging and discharging processes are assumed to be the same. The water flow rate is obtained setting a steam to carbon ratio equal to 1.25 [65] in the reformer.

Figure 8 represents the simplified functional scheme of the SOFC.

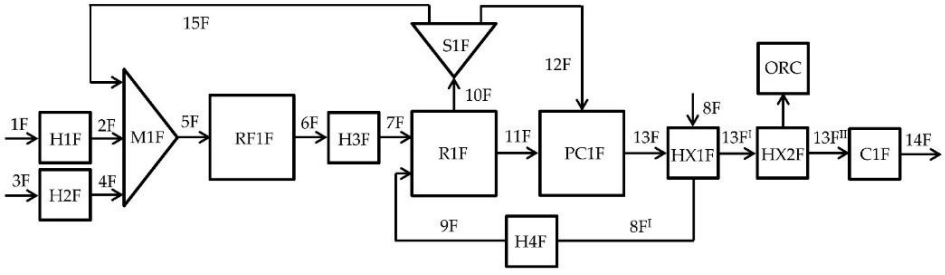

Fig. 8 – Simplified functional scheme of the SOFC section with thermal integrations (C = Cooler; H = Heater; HX = Heat exchanger; M = Mixer; PC = Post combustor; R = Reactor; RF = Reformer; S = Splitter)

386 The cell operates at ambient pressure. Methanol (1F) and water (3F) are vaporised (H1F and
387 H2F) and then mixed with a fraction of the high-temperature SOFC anode exhaust (15F),
388 allowing the mixture (5F) to reach the reforming temperature, set equal to 300 °C. Then,
389 following the methanol reforming reactions (RF1F) (opposite of the reactions (6)-(8)) a
390 hydrogen-rich mixture (6F, H_2 content approximately 64% by vol.) is obtained. The SOFC (R1F)
391 temperature is set equal to 850 °C, with a fuel utilisation factor of 0.85 [66]. The heat necessary
392 for the cell processes is obtained from the exothermic reaction in the cell itself. In particular,
393 methanol (H1F) and water (H2F) preheating and vaporisation, reforming reactions (RF1F),
394 reformed gas (H3F) and air (H4F) heating up to the cell temperature. The residual anode
395 exhaust gases (12F), mainly composed of H_2 and CO, are burnt in a post combustor (PC1F),
396 along with the air leaving the cathode (11F), increasing the exhaust temperature up to about
397 990 °C. The exhaust gases (13F) are firstly used to preheat (HX1F) the inlet air (8F) and then to
398 feed (HX2F) an ORC engine and improve the overall production of electricity during the
399 discharge phase.
400 Methanol and water preheating and vaporization require around 125 and 115 kW, respectively,
401 while the reforming reactions absorbs slightly more than 210 kW and the reformed gas requires
402 about 290 kW to be heated up to SOFC operating temperature. Since the total available thermal
403 power in the cell is equal to about 980 kW, a residual 235 kW is still available, allowing an
404 increase of the air temperature from about 760 °C to 850 °C. The air preheating from 25 to 760
405 °C requires about 1765 kW from the exhaust gases, leaving a further 700 kW available for
406 feeding the ORC engine.
407 Table 6 summarises the main parameters of the streams flowing through the SOFC depicted in
408 Fig. 8.
409

Table 6 – Mass flow, temperature and composition (by volume) of the main streams in the SOFC

	1F/2F	3F/4F	5F	6F	8F/9F	10F	11F	12F	13F/14F	15F
Mass flow [kg/s]	0.103	0.044	0.208	0.208	2.234	0.337	2.106	0.276	2.382	0.061
Temp [°C]	25/64	25/100	300	300	25/850	850	850	850	987/25	850

H_2	0.0000	0.0000	0.0306	0.6401	0.0000	0.0960	0.0000	0.0960	0.0000	0.0960
N_2	0.0000	0.0000	0.0000	0.0000	0.7728	0.0000	0.8152	0.0000	0.7063	0.0000
O_2	0.0000	0.0000	0.0000	0.0000	0.2074	0.0000	0.1639	0.0000	0.1325	0.0000
Ar	0.0000	0.0000	0.0000	0.0000	0.0092	0.0000	0.0097	0.0000	0.0084	0.0000
H_2O	0.0000	1.0000	0.4987	0.0943	0.0103	0.6384	0.0109	0.6384	0.1145	0.6384
CO	0.0000	0.0000	0.0119	0.0375	0.0000	0.0375	0.0000	0.0375	0.0001	0.0375
CO_2	0.0000	0.0000	0.0727	0.2281	0.0003	0.2281	0.0003	0.2281	0.0382	0.2281
CH_3OH	1.0000	0.0000	0.3861	0.0000	0.0000	0.0000	0.0000	0.0000	0.0000	0.0000

3.1.4. Organic Rankine cycle

Since there is a high residual thermal energy in the exhaust of the SOFC, it is possible to introduce an ORC in the system. Like steam plants, ORC systems are based on a Rankine cycle, but being the working fluid an organic compound rather than water, ORCs are capable to conveniently exploit even minor amount of heat available at low temperature (usually below 350 °C). An ORC is relatively simple being composed of an evaporator, a turbine, a condenser, a pump, and a regenerator [67]. A simplified functional scheme of the model of the ORC, as it was developed in Aspen Plus, is reported in Fig. 9.

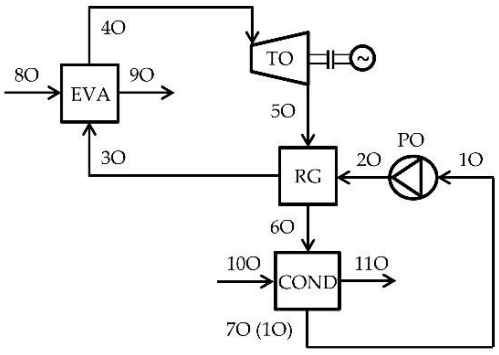

Fig. 9 – Simplified functional scheme of the organic Rankine cycle

The working fluid as saturated liquid (1O) is pumped (PO) to the maximum pressure of the cycle (2O). Then, it is preheated in a regenerator (RG) before entering an evaporator (EVA) where it is heated up to the maximum temperature of the cycle (4O) through the heat released by the cooling of the hot SOFC exhaust (8O). Then, the working fluid expands in a turbine (TO) producing electricity. The relatively high temperature of the turbine exhaust (5O) allows the

preheating of the working fluid (2O) in the regenerator (RG). Finally, exploiting cold water or air (10O), the working fluid (6O) condensate at the minimum pressure in the condenser (COND). Given the low temperature and mass flow of the available heat source (i.e. the hot gases coming from the SOFC section), this simple ORC configuration was chosen instead of a more complex layout (i.e. multi pressure level cycles, trilateral cycles, etc.).

Given the temperature of the hot source (about 380 °C), three potential working fluids were analysed, namely benzene, toluene, butylbenzene [68,69]. These three fluids are characterised by different properties as reported in Table 7. For each fluid, operating values of pressure and temperature are chosen to assure a complete vaporisation of the working fluid before entering the turbine.

Table 7 – ORC working fluids properties

Working fluid	T_{cr}	p_{cr}
Benzene	289 °C	48.9 bar
Toluene	320 °C	41.0 bar
Butylbenzene	387 °C	28.9 bar

A comparison between these working fluids was carried out. Benzene was found to provide the highest efficiency (consistently with Viktor et al. [69]), thanks to both its high critical pressure (48.9 bar) and low critical temperature (289 °C) [70].

Consequently, benzene was chosen as the organic fluid in this application. Even though benzene was chosen, it should be considered that it is a highly flammable and highly toxic compound that must be carefully handled and used [71]. Maximum cycle pressure and temperature were set to 46.5 bar and 289 °C. The pressure at the condenser was set slightly higher than 0.2 bar. A minimum temperature difference of 30 °C in the evaporator was set, leading to an outlet temperature of the hot source (9O) of about 115 °C. Globally, the ORC turbine produces about 210 kW, since the ORC harvests approximately 700 kW from the available hot source, and an ORC efficiency of about 0.30 was calculated.

3.2. System based on a reversible solid oxide cell

A configuration based on innovative technologies was considered for case B. In particular, the overall system is composed of three main sections:

- A high-temperature RSOC, operating both in electrolyser mode (SOEC) and fuel cell mode (SOFC), depending on RES availability;
- A methanol synthesis and purification section;
- A thermal energy storage system.

While the overall energy required by any electrolysis process to split water is almost constant, in high temperature processes (as in SOEC) the consumption of high-quality energy (i.e. electricity) remarkably decreases, so improving the efficiency in comparison to low-temperature ones. Conversely, in the SOEC the requirements of lower quality energy (i.e. heat) increases, necessitating an external source. Hence, the heat released by the SOFC exhaust can be accumulated in a TES system to be used during SOEC operation.

As assumed in the previous case, the RSOC-based system was sized considering a design power of the SOFC of 1 MW_e, requiring a methanol flow rate of approximately 370 kg/h. The flow rates of the main streams (namely air, water and CO_2) feeding the other sections were calculated to guarantee the desired methanol production.

3.2.1. Reversible solid oxide cells

As well as other equipment, the models of the RSOC were developed in Aspen Plus environment to simulate both the water splitting and the fuel oxidation. The model of the SOEC was derived from the one originally developed by Ni et al. [72]. The main difference with the model developed to simulate the SOFC regards the overvoltages, that in the SOEC are summed to the equilibrium voltage rather than subtracted, as shown by Eq. (11). More details on the parameters and on the model used to simulate the SOEC can be found in Lonis et al. [49].

$$E_{SOEC} = E_{eq} + [(\eta_{act} + \eta_{conc})_{an} + (\eta_{act} + \eta_{conc})_{cat} + \eta_{ohm}] \quad (11)$$

To avoid thermal management issues and material deterioration over time, the operating temperature of the RSOC (in both modes) was limited to 850 °C. The operating pressure was set equal to the ambient one. Indeed, high pressure brings about problems in the cells materials, and increases the complexity of the overall system, while reducing its reliability [73]. Moreover, high pressure can bring about premature break of the cells due to pressure gradients [74]. At the selected operating conditions, thermo-neutral operation is performed, avoiding external heat requirements.

Figure 10 represents the simplified functional scheme of the model developed in Aspen Plus.

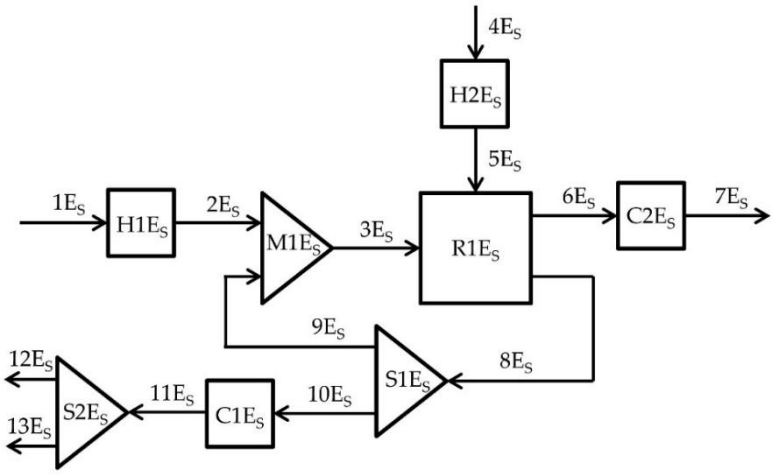

Fig. 10 – Simplified functional scheme of the solid oxide electrolyser section (C = Cooler; H = Heater; M = Mixer; R = Reactor; S = Splitter)

On the cathode side, the water ($1E_S$) preheating, vaporisation and superheating ($H1E_S$) take place. Since a feed composition of 90% water, 10% hydrogen ([75]) is set for the cell, a fraction of the cathode exhaust ($9E_S$) is mixed ($M1E_S$) with the vapour ($2E_S$). Then, the mixture is electrolysed in the reactor ($R1E_S$) and hydrogen and oxygen are produced. On the anode side, the sweep air ($4E_S$) is heated ($H2E_S$) from ambient temperature up to 850 °C. Both the hydrogen-water mixture ($10E_S$) and the outlet air ($6E_S$) are cooled to ambient temperature and the released heat is recovered to reduce the overall thermal energy requirement of the SOEC. Since a water utilisation factor of 0.85 is assumed, a water flowrate of 780 kg/h is required to produce the hydrogen for the MSS (76 kg/h). The SOEC requires an electric power of approximately 2.5 MW_e.

Table 8 summarises the mass flow rate, temperature, and molar fraction of the main streams depicted in the simplified scheme of Fig. 10.

Table 8 – Mass flow, temperature and composition (by volume) of the main streams in the SOEC

	$1E_S/2E_S$	$3E_S$	$4E_S/5E_S$	$6E_S/7E_S$	$8E_S$	$9E_S$	$10E_S/11E_S$	$12E_S$
Mass flow [kg/s]	0.217	0.224	0.236	0.403	0.057	0.0066	0.0503	0.021
Temp [°C]	25/850	850	25/850	850/25	850	850	850/25	25
H_2	0.0000	0.1000	0.0000	0.0000	0.8650	0.8650	0.8650	1.0000
N_2	0.0000	0.0000	0.7728	0.4724	0.0000	0.0000	0.0000	0.0000
O_2	0.0000	0.0000	0.2073	0.5155	0.0000	0.0000	0.0000	0.0000
Ar	0.0000	0.0000	0.0092	0.0056	0.0000	0.0000	0.0000	0.0000
H_2O	1.0000	0.9000	0.0103	0.0063	0.1350	0.1350	0.1350	0.0000
CO_2	0.0000	0.0000	0.0003	0.0002	0.0000	0.0000	0.0000	0.0000

The SOEC performance was improved through an internal heat recovery. Figure 11 shows the simplified functional scheme of the SOEC section with thermal integration.

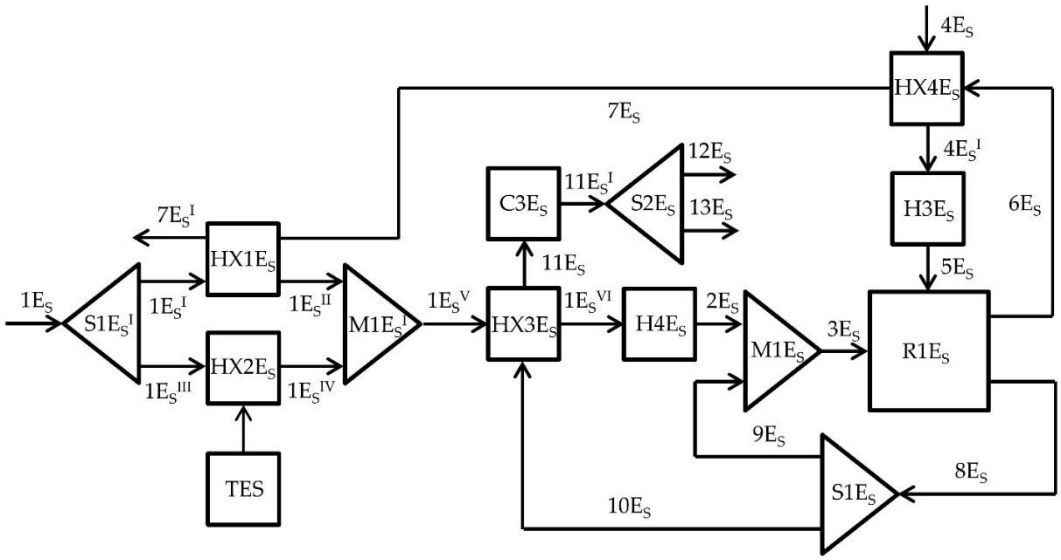

Fig. 11 – Simplified functional scheme of the SOEC section with thermal integrations (C = Cooler; H = Heater; HX = Heat exchanger; M = Mixer; R = Reactor; S = Splitter)

On the anode side, the hot (850 °C) exhausts ($6E_S$) preheat the sweep air ($4E_S$) up to 800 °C in $HX4E_S$ (setting to 50 °C the minimum temperature difference between the hot inlet and the cold outlet). Coupling the cold sweep air to the anode exhaust allows the recovery of approximately 200 kW. In addition, to complete the heating process of the sweep air a further 15 kW must be provided by an additional heater ($H3E_S$). Since the anode exhaust ($6E_S$) is composed of both the sweep air and the oxygen produced in the SOEC, preheating the sole sweep air cools it

down just to about 405 °C ($7E_S$), allowing a further heat recovery. On the cathode side, the water ($1E_S$) is preheated, vaporized and superheated through two different sources. A fraction of the water flow rate ($1E_S^I$, about 185 out of the total 780 kg/h) is preheated and vaporized in $HX1E_S$ exploiting the residual heat of the hot anode exhaust ($7E_S$). The remainder ($1E_S^{III}$) is preheated and vaporized in $HX2E_S$ by harvesting the heat stored in the TES system during discharge mode operation of the RSOC. Approximately 425 kW are recovered with this integration. Then, the saturated water vapour is superheated ($HX3E_S$) to about 680 °C exploiting the hot cathode exhaust ($10E_S$, composed of hydrogen and water), saving approximately 260 kW. An external heater ($H4E_S$) is still required to reach the SOEC operating temperature (850 °C), absorbing a power of 85 kW. In addition, as previously specified, a portion of the cathode exhaust ($9E_S$) is recycled to the reactor ($R1E_S$) inlet.

Table 9 summarises the energy balances of the heating and cooling processes within the SOEC system.

Table 9 – Main heat transfers in the SOEC

Heating process	Heat [kW]	Cooling process	Heat [kW]
Sweep air PH by heat recovery ($HX4E_S$)	197.8	Anode exhaust 1st cooling ($HX4E_S$)	-197.8
Sweep air PH by external source ($H3E_S$)	13.8	Anode exhaust 2nd cooling ($HX1E_S$)	-133.9
Water PH and VAP by heat recovery ($HX1E_S$)	133.9	Cathode exhaust 1st cooling ($HX3E_S$)	-260.8
Water PH and VAP by external source or TES ($HX2E_S$)	426.6	Cathode exhaust 2nd cooling ($C3E_S$)	-101.2
Steam SH by heat recovery ($HX3E_S$)	260.8		
Steam SH by external source ($H4E_S$)	84.5		

PH: preheating; VAP: vaporisation; SH: superheating

3.2.2. MSS and SOFC (RSOC)

The MSS in the RSOC-based system differs from the one in the AEL-based system only regarding the hydrogen compression train. Indeed, since the RSOC operates at ambient pressure, the produced hydrogen must be compressed from 1 to 65 bar. Consequently, In the

RSOC-based system, three compressors with an intercooling temperature of 38 °C and a compression ratio of 4.02 were considered for both the hydrogen and the CO_2.

The SOFC section is almost identical to that of the AEL-based configuration, so no further information is provided here. The only difference is that the thermal energy of the SOFC exhaust does not feed an ORC, but it is stored in a TES system and used subsequently to vaporise the water in the electrolyser during the charge mode. A thermal power equal to 425 kW must be stored in the TES system during SOFC operation to complete the water vaporisation process during SOEC operation (Table 9, $HX2E_S$). The remaining thermal energy would be scarce and available at low temperature, so the possibility of feeding an ORC was not contemplated in this configuration.

3.2.3. Thermal energy storage system

Among different technologies, in this study, a latent heat thermal energy storage (LHTES) system based on a tank filled by a phase change material (PCM) was chosen to transfer thermal energy from the RSOC in SOFC-mode to the RSOC in SOEC-mode.

Figure 12 shows a simplified scheme of the thermal energy storage section with the interactions between the TES and a gas-water heat exchanger (GWHX).

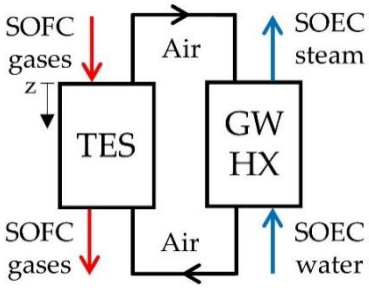

Fig. 12 – Thermal energy storage system detail

During the TES charging phase, the hot exhausts from the SOFC enter from the top of the TES, releasing thermal energy to the PCM that melts. Then the hot exhausts leave the bed from the bottom of the tank. Conversely, during the TES discharging phase, the direction of the flow is reversed, recovering the heat from the PCM. The air, used as an intermediate heat transfer fluid, circulates in a closed loop and, inside the GWHX, it releases the heat gained from the TES to the water feeding the SOEC. Approximately 50 kW are necessary to vent the air in the circuit.

The LHTES was preliminary designed through a numerical simulation model developed in MATLAB-Simulink and based on a transient one-dimensional (1-D) two-equation model (LTNE). The optimal size and configuration of the TES and the thermal behaviour of the storage unit can be found analysing and calculating the temperature profile of both the heat thermal fluid (HTF) and of the PCM. The single tank, based on a packed bed configuration, is assumed to be filled by a PCM held in capsules 50 mm in diameter. The bed is assumed to be porous, homogeneous and isotropic, with negligible energy losses, while the radial temperature profile is set constant to calculate the shape of the thermocline along the bed. A detailed description of the developed model can be found in previous papers by the same authors [76,77].

Given the initial temperature of the hot source (about 380 °C), sodium hydroxide (NaOH) contained in stainless steel [78–80] was identified as a suitable PCM for this application. The phase change temperature of the NaOH is equal to 318 °C, the latent heat of fusion to 165 $\mathrm{kJ/kg}$ and the mean density is 2100 $\mathrm{kg/m^3}$ [81]. A deeper analysis of this TES system is reported in [82].

3.3. Performance indices

Several performance indices were developed to study and compare the two different analysed systems. In particular, performance indices were defined for each section consistently with respect to the interrelationships between the various sections and to the overall system.

In this sense, the efficiency of the electrolyser η_{ele}, valid for both the alkaline electrolyser and the solid oxide one, is defined by Eq. (12):

$$\eta_{ele} = \frac{\dot{m}_{H_2} \cdot LHV_{H_2}}{P_{ele} + P_{BOP,ele}} \tag{12}$$

where $\dot{m}_{H_2}$ is the hydrogen flow rate while LHV_{H_2} is the lower heating value, P_{ele} is the power consumption of the electrolyser, and $P_{BOP,ele}$ is the auxiliaries electrical requirements, respectively.

The SOFC efficiency η_{SOFC} is defined by Eq. (13), considering the net power of the SOFC and the chemical power of the methanol entering the section $\dot{m}_{MeOH} \cdot LHV_{MeOH}$:

$$\eta_{SOFC} = \frac{P_{SOFC} - P_{BOP,SOFC}}{\dot{m}_{MeOH} \cdot LHV_{MeOH}} \quad (13)$$

566 The efficiency of the MSS is defined by Eq. r:

$$\eta_{MSS} = \frac{\dot{m}_{MeOH} \cdot LHV_{MeOH}}{\dot{m}_{H_2} \cdot LHV_{H_2} + \dot{E}_{MSS} + P_{BOP,MSS}} \quad (14)$$

567 in which the term $\dot{E}_{MSS}$ is the external supply for H2 and CO2 preheating, while the term
568 $P_{BOP,MSS}$ is the auxiliaries requirement.

569 A chemical energy conversion efficiency of the MSS can also be defined similarly to a “cold gas”
570 efficiency of a gasifier, that is the ratio between the chemical power of the methanol and the
571 chemical power of the hydrogen, as reported in Eq. (15):

$$\eta_{MSS,C} = \frac{\dot{m}_{MeOH} \cdot LHV_{MeOH}}{\dot{m}_{H_2} \cdot LHV_{H_2}} \quad (15)$$

572 A global efficiency η_G can be defined for the overall system according to Eq. (16):

$$\eta_G = \frac{P_{SOFC} - P_{BOP,SOFC}}{P_{ele} + P_{BOP,ele} + \dot{E}_{MSS} + P_{BOP,MSS}} \quad (16)$$

573 The global efficiency can be also obtained by the following Eq. (17), by combining Eq. (16) with
574 Eqs. (12), (13) and (15) and rearranging the various terms:

$$\eta_G = \eta_{ele} \cdot \eta_{SOFC} \cdot \eta_{MSS,C} \cdot \varphi_{ele} \quad (17)$$

575 being:

$$\varphi_{ele} = \frac{P_{ele} + P_{BOP,ele}}{P_{ele} + P_{BOP,ele} + \dot{E}_{MSS} + P_{BOP,MSS}} \quad (18)$$

576 where φ_{ele} represents ratio between the power supply of the electrolyser and the total power
577 required by the overall system.

578 A further alternative expression of the global efficiency, as reported by Eq. (19), can be obtained
579 by combining Eq. (17) with Eq. (14):

$$\eta_G = \eta_{ele,R} \cdot \eta_{SOFC} \cdot \eta_{MSS} \quad (19)$$

580 where $\eta_{ele,R}$ is a rectified efficiency of the electrolyser given by Eq. (20):

$$\eta_{ele,R} = \frac{\dot{m}_{H_2} \cdot LHV_{H_2} + (\dot{E}_{MSS} + P_{BOP,MSS})}{P_{ele} + P_{BOP,ele} + (\dot{E}_{MSS} + P_{BOP,MSS})} \quad (20)$$

581 Obviously, the rectified efficiency of the electrolyser $\eta_{ele,R}$ coincides with the efficiency η_{ele} when
582 the MSS does not require an external power supply. By the way, it can be observed that adding
583 the same quantity $(\dot{E}_{MSS} + P_{BOP,MSS})$ to numerator and denominator in Eq. (15), results $\eta_{ele,R} >$
584 η_{ele}.
585 Furthermore, the correlation between the relevant efficiency parameters of the comprehensive
586 electrolyser-MSS system is highlighted in the following Eq. (21), by combining Eqs. (17) and
587 (19):

$$\eta_{ele} \cdot \varphi_{ele} \cdot \eta_{MSS,C} = \eta_{ele,R} \cdot \eta_{MSS} \quad (21)$$

588 Finally, a power-to-liquid efficiency η_{PtL} is defined by Eq. (22):

$$\eta_{PtL} = \frac{\dot{m}_{MeOH} \cdot LHV_{MeOH}}{P_{ele} + P_{BOP,ele} + \dot{E}_{MSS} + P_{BOP,MSS}} \quad (22)$$

589 In case of RSOC-based configuration, the presence of the ORC brings about a variation in the
590 efficiency of the power production section $\eta_{SOFC+ORC}$ and of the global efficiency η_G. The
591 modified equations are (23) and (24):

$$\eta_{SOFC+ORC} = \frac{P_{SOFC} - P_{BOP,SOFC} + P_{ORC} - P_{BOP,ORC}}{\dot{m}_{MeOH} \cdot LHV_{MeOH}} \quad (23)$$

592

$$\eta_G = \frac{P_{SOFC} - P_{BOP,SOFC} + P_{ORC} - P_{BOP,ORC}}{P_{ele} + P_{BOP,ele} + \dot{E}_{MSS} + P_{BOP,MSS}} \quad (24)$$

593 The terms P_{ORC} and $P_{BOP,ORC}$ are the electric power produced by the ORC and its balance of
594 plant, respectively.
595 The values of the terms used to calculate the performance indices previously described for both
596 the AEL-based system and the RSOC-based system. are reported in Table 10.

Table 10 – Main results of the AEL-based and RSOC-based systems

AEL-based			SOEC-based		
Section	Process	Power [kW]	Section	Process	Power [kW]
AEL	P_{AEL}	3453	SOEC	P_{SOEC}	2528
	$\dot{m}_{H_2} \cdot LHV_{H_2}$	2520		$\dot{m}_{H_2} \cdot LHV_{H_2}$	2520
	$P_{BOP,AEL}$	0.7		$P_{BOP,SOEC}$	98.3
Methanol synthesis	$\dot{m}_{MeOH} \cdot LHV_{MeOH}$	2033	Methanol synthesis	$\dot{m}_{MeOH} \cdot LHV_{MeOH}$	2033
	$\dot{m}_{H_2} \cdot LHV_{H_2}$	2520		$\dot{m}_{H_2} \cdot LHV_{H_2}$	2520
	$P_{BOP,MSS}$	93.5		$P_{BOP,MSS}$	239
	$\dot{E}_{MSS}$	0		$\dot{E}_{MSS}$	0
SOFC	P_{SOFC}	1000	SOFC	P_{SOFC}	1000
	$\dot{m}_{MeOH} \cdot LHV_{MeOH}$	2033		$\dot{m}_{MeOH} \cdot LHV_{MeOH}$	2033
	$P_{BOP,SOFC}$	0		$P_{BOP,SOFC}$	50
ORC	P_{ORC}	210.4		/	/
	$P_{BOP,ORC}$	7.2		/	/

Given the low operating temperature of the AEL, the power consumed to perform the electrolysis is almost 1 MW higher than that consumed in the SOEC, because the latter operates at high temperature and a remarkable portion of the required heat is provided by the TES charged during SOFC operation. Given the considerations on the design and sizing of the system, the hydrogen and methanol chemical power are the same in both the AEL and the SOEC-based systems, as well as the power entering (chemical) and produced (electrical) by the SOFC. In both cases, the MSS external energy term $\dot{E}_{MSS}$ is zero because it was possible, with a wise exploitation of the heat available within the section, to make the MSS self-sustainable.

4. Overall systems performance and comparison

Table 11 summarises the performance indices of each section and of the overall system for both studied configurations.

Table 11 – Comparison of the main performance indices of the studied configurations

Efficiency	AEL (w/ ORC)	RSOC (w/ TES)
η_{ele}	0.730	0.960
η_{MSS}	0.778	0.737
η_{PtL}	0.573	0.710
$\eta_{SOFC}/\eta_{SOFC+ORC}$	0.592	0.467
η_{G}	0.339	0.332

Comparison of the auxiliay performance indices of the studied configurations

Efficiency	AEL (w/ ORC)	RSOC (w/ TES)
$\eta_{MSS,C}$	0.807	0.807
φ_{ele}	0.974	0.917
$\eta_{ele,R}$	0.737	0.963

As it was expected, the electrolyser based on solid oxide cells showed a higher efficiency (0.960) than the alkaline one (0.730), thanks to the high operating temperature that allows for lower electricity consumption. The efficiency of the methanol synthesis section resulted larger in the AEL-based system because the electrolyser operates at high pressure (25 bar), reducing both the number of compressors in the MSS and the total power consumption, saving more than 70 kW. Despite a lower MSS efficiency, since the power-to-liquid efficiency is directly related to the efficiencies of both the electrolyser and the MSS, its value is higher for the RSOC-based system (0.710 vs 0.573), because the electrolyser efficiency η_{ele} is significantly higher than that of the AEL. Since the introduction of the ORC increases the power production of about 20%, $\eta_{SOFC+ORC}$ in the AEL-based system is remarkably higher (0.592) than the corresponding η_{SOFC} (0.467) in the RSOC-based system. Finally, even though the efficiency of the SOEC is significantly larger than that of the AEL, the two configurations show similar global efficiencies.

623 In particular, the global efficiency of the AEL-based system (0.339) is only 0.7 percentage point
624 higher than that of the AEL-based system (0.332).

625 ## 5. Conclusion

626 Given the rising climate challenge related to CO_2 emissions, power-to-X processes are an
627 interesting solution to reduce the overall emissions of CO_2 in the atmosphere, by exploiting
628 renewable energy to produce different types of chemicals compounds to be used as fuels or as
629 chemicals in the industry. Coupling renewable H_2 production with recycled CO_2 could be
630 employed to create a closed carbon cycle where the CO_2 in atmosphere is used to build carbon-
631 based compounds.
632 In this paper, two different integrated energy systems for the production and use of renewable
633 methanol through water electrolysis and CO_2 hydrogenation were analysed and compared. In
634 the first, the water electrolysis is carried out in an AEL coupled to a methanol synthesis section
635 to produce clean methanol to be stored and then used in a SOFC. In the second, the system
636 was supposed to be based on a high temperature reversible solid oxide cell (RSOC), capable of
637 operating alternatively as an SOEC and as an SOFC, reducing the number of components.
638 In the case of the AEL-based plant, an ORC was also introduced to boost the electricity, while in
639 the case of the RSOC-based system, a TES was considered to recover waste heat during
640 discharge mode and provide it during charge mode. Several coherent performance indices were
641 specifically defined to compare the two overall systems and their subsections.
642 The system was sized to produce a power of 1 MW in fuel cell operation, requiring a power of
643 about 3.5 MW in case of AEL and 2.5 MW for the SOEC. The introduction of the ORC leads to
644 an increase of the overall electricity production of 210 kW, whereas the TES allows the recovery
645 of 425 kW of heat, reducing SOEC requirements. The efficiency calculated for the AEL (0.73),
646 the SOEC (0.96) and the SOFC (0.47), as well as the power-to-liquid efficiency (ranging from
647 0.57 to 0.71), are consistent with literature data. The global efficiency of the two systems was
648 almost the same, with the AEL-based system characterised by a slightly higher efficiency
649 (0.339) than the RSOC-based system (0.332).

Since the difference between the two configurations is minor, other aspects should be taken into account. For instance, the solid oxide cells (SOEC/SOFC) and the alkaline cells are not at the same technology readiness level (TRL [83]). While the former is still not commercially mature with a TRL of 6-7, and is expected to reach a TRL of 9 by the 2030 [84], the latter is already largely diffused and commercially available. However, since also the power-to-methanol process employing captured CO_2 and renewable energy is at a TRL of 6-7 [85], a binary technological improvement of the solid oxide cells and renewable power-to-methanol technologies might be expected, leading to a harmonised progress of both the single technologies and the overall system.

Another aspect to be considered, but not investigated in this paper, is related to the costs of the PtL technologies. Indeed, the main drawback of such systems consists of their high cost, due to the electricity production from RES and the capital cost of the electrolysers. For instance, SOEC methanol production processes are approximately 15 times more expensive than conventional methanol production from fossil fuels [37]. In addition, even though RES is becoming more convenient than conventional electricity production, the costs related to the electrolysers, both AEL and SOEC/RSOC technology, remains remarkably large. Schimdt et al [38] provided a capital cost estimation of 1000-1200 €/kW for the AEL and higher than 2000 €/kW for the SOEC technology. Nonetheless, in a future perspective these costs are expected to drop sensibly [37–40]. In addition, a large reduction in SOC costs is expected, with values comparable to those of alkaline and PEM cells by 2030 [37,38]. Pérez-Fortes et al. [86] analysed a methanol production facility that recycles CO_2 from a conventional power plant using conventional CCU technology. The system resulted economically unfeasible owing to the high costs of H_2 production and CO_2 capture with the available technology. Hence, the feasibility of the production of methanol from these raw materials is directly related to the development of the technologies used to gather the feedstock. Clearly, if a serious R&D effort is put into the technological progress on this fields, the costs might be lowered enough to guarantee the economic feasibility of this methanol production approach.

Nowadays, even though the costs of renewable methanol production are still too high to represent a competitive and feasible solution to the climate change, such a technology would play a fundamental role in the decarbonisation of society. Indeed, it is difficult to imagine a complete desertion of the conventional fuel technologies in the short period. Indeed, the use of liquid and gaseous fuels should still be expected for many years from now. For instance, renewable methanol might be used, as already happens in Iceland, to fuel vehicles with a net CO_2 emission equal to zero while using existing technologies (internal combustion engines or fuel cells). This solution, in the long term, is more sustainable than substituting all vehicles with electric alternatives.

Finally, the CCU application analysed in this work and in numerous other studies, should be used side by side with CCS technologies, to both create a closed carbon cycle (avoiding the emission of new carbon in the atmosphere) and reduce the overall amount of CO_2 in the atmosphere.

Acknowledgment

The Research Project was supported by “Fondazione di Sardegna”, CRP project F71I170002800.

Francesco Lonis also gratefully acknowledges Sardinia Regional Government for the financial support for his Ph.D. scholarship (P.O.R. Sardegna F.S.E. Operational Programme of the Autonomous Region of Sardinia, European Social Fund 2014-2020 - Axis III Education and Training, Thematic Goal 10, Specific goal 10.5, Action partnership agreement 10.5.12).

Bibliography

[1] Power-to-X | Energy Topics | Siemens n.d. https://new.siemens.com/global/en/products/energy/topics/power-to-x.html (accessed January 17, 2020).

[2] Offermanns H, Plass L, Bertau M. Introduction. In: Bertau M, Offermanns H, Plass L, Schmidt F, Wernicke H-J, editors. Methanol Basic Chem. Energy Feed. Futur. Asinger’s Vis. Today, Berlin, Heidelberg: Springer Berlin Heidelberg; 2014, p. 1–22. doi:10.1007/978-3-642-39709-7_1.

[3] Blanco H, Nijs W, Ruf J, Faaij A. Potential for hydrogen and Power-to-Liquid in a low-carbon EU energy system using cost optimization. Appl Energy 2018;232:617–39. doi:10.1016/j.apenergy.2018.09.216.

[4] Olah GA, Goeppert A, Prakash GKS. Chemical recycling of carbon dioxide to methanol and dimethyl ether: From greenhouse gas to renewable, environmentally carbon neutral fuels and synthetic hydrocarbons. J Org Chem 2009;74:487–98. doi:10.1021/jo801260f.

[5] Sternberg A, Bardow A. Power-to-What?-Environmental assessment of energy storage systems. Energy Environ Sci 2015;8:389–400. doi:10.1039/c4ee03051f.

[6] Power-To-X: Entering the Energy Transition with Kopernikus - RWTH AACHEN UNIVERSITY - English n.d. https://www.rwth-aachen.de/go/id/kvyv/lidx/1 (accessed January 17, 2020).

[7] Bossmann T, Fournié L, Humberset L, Khallouf P. METIS Study S8 - The role and potential of Power-to-X in 2050. 2018. doi:10.2833/459958.

[8] Galindo Cifre P, Badr O. Renewable hydrogen utilisation for the production of methanol.

719 Energy Convers Manag 2007;48:519–27. doi:10.1016/j.enconman.2006.06.011.
720 [9] Power-to-X solutions. Innov Landsc a Renewable-Powered Futur Solut to Integr Var
721 Renewables 2019:1–8. https://irena.org/-/media/Files/IRENA/Agency/Topics/Innovation-and-
722 Technology/IRENA_Landscape_Solution_11.pdf?la=en&hash=2BE79AC597ED18A96E541
723 5942E0B93232F82FD85 (accessed November 9, 2019).
724 [10] Pflug V, Zindel E, Zimmermann G, Olvera OR, Pyc I, Trulley C. Power-to-X: The crucial
725 business on the way to a carbon-free world. Tech Pap Siemens AG 2019:1–26.
726 [11] Salpakari J, Mikkola J, Lund PD. Improved flexibility with large-scale variable renewable
727 power in cities through optimal demand side management and power-to-heat conversion.
728 Energy Convers Manag 2016;126:649–61. doi:10.1016/j.enconman.2016.08.041.
729 [12] Bloess A, Schill WP, Zerrahn A. Power-to-heat for renewable energy integration: A review of
730 technologies, modeling approaches, and flexibility potentials. Appl Energy 2018;212:1611–
731 26. doi:10.1016/j.apenergy.2017.12.073.
732 [13] Schmidt P, Batteiger V, Roth A, Weindorf W. Power-to-Liquids as Renewable Fuel Option
733 for Aviation : A Review 2018:127–40. doi:10.1002/cite.201700129.
734 [14] Schemme S, Can R, Peters R, Stolten D. Power-to-fuel as a key to sustainable transport
735 systems – An analysis of diesel fuels produced from CO2 and renewable electricity. Fuel
736 2017;205:198–221. doi:10.1016/j.fuel.2017.05.061.
737 [15] Pozzo M, Lanzini A, Santarelli M. Enhanced biomass-to-liquid (BTL) conversion process
738 through high temperature co-electrolysis in a solid oxide electrolysis cell (SOEC). Fuel
739 2015;145:39–49. doi:10.1016/j.fuel.2014.12.066.
740 [16] Hillestad M, Ostadi M, Alamo G, Rytter E, Austbø B, Pharoah JG. Improving carbon
741 efficiency and profitability of the biomass to liquid process with hydrogen from renewable
742 power. Fuel 2018;234:1431–51. doi:10.1016/j.fuel.2018.08.004.
743 [17] Bergins C, Tran KC, Wu S, Kakaras E, Buddenberg T, Sigurbjörnsson Ó, et al. The
744 Challenge of Energy Storage in Europe: Focus on Power to Fuel. J Energy Resour Technol
745 2016;138:042002. doi:10.1115/1.4032544.
746 [18] Bassano C, Deiana P, Lietti L, Visconti CG. P2G movable modular plant operation on
747 synthetic methane production from CO2 and hydrogen from renewables sources. Fuel
748 2019;253:1071–9. doi:10.1016/j.fuel.2019.05.074.
749 [19] de Vasconcelos BR, Lavoie JM. Recent advances in power-to-X technology for the
750 production of fuels and chemicals. Front Chem 2019;7:1–24.
751 doi:10.3389/fchem.2019.00392.
752 [20] Bertau M, Offermanns H, Plass L, Schmidt F. Methanol: The Basic Chemical and Energy
753 Feedstock of the Future. 2014. doi:10.1007/978-3-642-39709-7.
754 [21] Methanol Institute. Energy - Methanol Institute 2010. http://www.methanol.org/energy/
755 (accessed July 24, 2018).
756 [22] Baak JA, Pozarlik AK, Arentsen MJ, Brem G. Techno-economic study of a zero-emission
757 methanol based energy storage system. Energy Convers Manag 2019;182:530–45.
758 doi:10.1016/j.enconman.2018.12.015.
759 [23] Ganesh I. Conversion of carbon dioxide into methanol - A potential liquid fuel: Fundamental
760 challenges and opportunities (a review). Renew Sustain Energy Rev 2014;31:221–57.
761 doi:10.1016/j.rser.2013.11.045.
762 [24] Mignard D, Pritchard C. Processes for the Synthesis of Liquid Fuels from CO2 and Marine
763 Energy. Chem Eng Res Des 2006;84:828–36. doi:10.1205/cherd.05204.
764 [25] O'Brien JE, McKellar MG, Stoots CM, Herring JS, Hawkes GL. Parametric study of large-
765 scale production of syngas via high-temperature co-electrolysis. Int J Hydrogen Energy
766 2009;34:4216–26. doi:10.1016/j.ijhydene.2008.12.021.
767 [26] Graves C, Ebbesen SD, Mogensen M, Lackner KS. Sustainable hydrocarbon fuels by
768 recycling CO2 and H2O with renewable or nuclear energy. Renew Sustain Energy Rev
769 2011;15:1–23. doi:10.1016/j.rser.2010.07.014.
770 [27] Crivellari A, Cozzani V, Dincer I. Design and energy analyses of alternative methanol
771 production processes driven by hybrid renewable power at the offshore Thebaud platform.
772 Energy Convers Manag 2019;187:148–66. doi:10.1016/j.enconman.2019.03.017.
773 [28] Albrecht FG, Konig DH, Dietrich RU. The potential of using power-to-liquid plants for power
774 storage purposes. Int Conf Eur Energy Mark EEM 2016;2016–July.

775 doi:10.1109/EEM.2016.7521203.
776 [29] Albrecht F, Estelmann S, Dietrich R. Technical Economic Evaluation of Renewable Jet Fuel
777 from Power, Biomass and/or Carbon Dioxide. 4th Eur Refin Technol Conf 2017.
778 [30] Albrecht FG, König DH, Baucks N, Dietrich R. A standardized methodology for the techno-
779 economic evaluation of alternative fuels – A case study. Fuel 2017;194:511–26.
780 doi:10.1016/j.fuel.2016.12.003.
781 [31] Fasihi M, Bogdanov D, Breyer C. Techno-Economic Assessment of Power-to-Liquids (PtL)
782 Fuels Production and Global Trading Based on Hybrid PV-Wind Power Plants. Energy
783 Procedia 2016;99:243–68. doi:10.1016/j.egypro.2016.10.115.
784 [32] Schmidt P, Weindorf W, Roth A, Batteiger V, Riegel F. Power-to-Liquids Potentials and
785 Perspectives for the Future Supply of Renewable Aviation Fuel 2016:32.
786 [33] Michailos S, McCord S, Sick V, Stokes G, Styring P. Dimethyl ether synthesis via captured
787 CO2 hydrogenation within the power to liquids concept: A techno-economic assessment.
788 Energy Convers Manag 2019;184:262–76. doi:10.1016/j.enconman.2019.01.046.
789 [34] Hansen JB, Topsøe H. The CO2 Electrofuel Project 2015.
790 [35] IRENA. Renewable Power Generation Costs in 2017. IRENA - International Renewable
791 Energy Agency. 2018.
792 [36] Lazard. Levelized Cost of Energy Analysis 2018. 2018.
793 [37] Rivera-Tinoco R, Farran M, Bouallou C, Auprêtre F, Valentin S, Millet P, et al. Investigation
794 of power-to-methanol processes coupling electrolytic hydrogen production and catalytic CO2
795 reduction. Int J Hydrogen Energy 2016;41:4546–59. doi:10.1016/j.ijhydene.2016.01.059.
796 [38] Schmidt O, Gambhir A, Staffell I, Hawkes A, Nelson J, Few S. Future cost and performance
797 of water electrolysis : An expert elicitation study. Int J Hydrogen Energy 2017;42:30470–92.
798 doi:10.1016/j.ijhydene.2017.10.045.
799 [39] Hank C, Gelpke S, Schnabl A, White RJ, Full J, Wiebe N, et al. Economics & carbon dioxide
800 avoidance cost of methanol production based on renewable hydrogen and recycled carbon
801 dioxide – power-to-methanol. Sustain Energy Fuels 2018:1244–61.
802 doi:10.1039/C8SE00032H.
803 [40] Akikur RK, Saidur R, Ping HW, Ullah KR. Performance analysis of a co-generation system
804 using solar energy and SOFC technology. Energy Convers Manag 2014;79:415–30.
805 doi:10.1016/j.enconman.2013.12.036.
806 [41] Methanol - Clean Energy | Methanol Institute n.d. https://www.methanol.org/energy/
807 (accessed May 2, 2019).
808 [42] Faberi S, Paolucci L. Methanol : a future transport fuel based on hydrogen and carbon
809 dioxide. 2014. doi:10.2861/57305.
810 [43] Olah GA, Goeppert A, Prakash GKS. Beyond Oil and Gas: The Methanol Economy. 2nd ed.
811 Weinheim, Germany: Wiley-VCH Verlag GmbH & Co. KGaA; 2009.
812 doi:10.1002/9783527627806.
813 [44] Olah GA. Towards oil independence through renewable methanol chemistry. Angew
814 Chemie - Int Ed 2013;52:104–7. doi:10.1002/anie.201204995.
815 [45] CRI - Carbon Recycling International n.d. https://www.carbonrecycling.is/home (accessed
816 December 18, 2019).
817 [46] Carbon Recycling International | below50 n.d. https://below50.org/project/carbon-recycling-
818 international/ (accessed May 14, 2018).
819 [47] Bergins C, Fox EL, Tran KC, Wuebben P. Commercialization of Low Carbon Methanol.
820 Fuels Lubr Futur 2016:22–5. doi:10.1007/s40111-015-0517-0.
821 [48] Bergins C, Tran K, Koytsoumpa E, Kakaras E, Buddenberg T, Sigurbjörnsson Ó. Power to
822 Methanol Solutions for Flexible and Sustainable Operations in Power and Process
823 Industries. Power-Gen Eur 2015.
824 [49] Lonis F, Tola V, Cau G. Renewable methanol production and use through reversible solid
825 oxide cells and recycled CO2 hydrogenation. Fuel 2019;246:500–15.
826 doi:10.1016/j.fuel.2019.02.108.
827 [50] Minh NQ, Mogensen MB. Reversible Solid Oxide Fuel Cell Technology for Green Fuel and
828 Power Production. Interface Mag 2013;22:55–62. doi:10.1149/2.F05134if.
829 [51] Mermelstein J, Posdziech O. Development and Demonstration of a Novel Reversible SOFC
830 System for Utility and Micro Grid Energy Storage. Fuel Cells 2017;17:562–70.

831 doi:10.1002/fuce.201600185.
832 [52] Sapountzi FM, Gracia JM, Weststrate CJ (Kees-J, Fredriksson HOA, Niemantsverdriet JW
833 (Hans). Electrocatalysts for the generation of hydrogen, oxygen and synthesis gas. Prog
834 Energy Combust Sci 2017;58:1–35. doi:10.1016/j.pecs.2016.09.001.
835 [53] Wang Y, Banerjee A, Wehrle L, Shi Y, Brandon N, Deutschmann O. Performance analysis
836 of a reversible solid oxide cell system based on multi-scale hierarchical solid oxide cell
837 modelling. Energy Convers Manag 2019;196:484–96. doi:10.1016/j.enconman.2019.05.099.
838 [54] EG&G Technical Services I. Fuel Cell Handbook. 7th ed. U.S. Department of Energy; 2004.
839 [55] Ni M, Zhao TS, editors. Solid Oxide Fuel Cells: From Materials to System Modeling.
840 Cambridge: The Royal Society of Chemistry; 2013. doi:10.1039/9781849737777.
841 [56] Berkeley L. Sunfire SOEC steam electrolysis module for Salzgitter Flachstahl. Fuel Cells
842 Bull 2017;2017:12. doi:10.1016/s1464-2859(17)30269-9.
843 [57] Minh NQ. Solid oxide fuel cells for power generation and hydrogen production. J Korean
844 Ceram Soc 2010;47:1–7. doi:10.4191/KCERS.2010.47.1.001.
845 [58] Zeng K, Zhang D. Recent progress in alkaline water electrolysis for hydrogen production
846 and applications. Prog Energy Combust Sci 2010;36:307–26.
847 doi:10.1016/j.pecs.2009.11.002.
848 [59] Ursua A, Sanchis P. Static-dynamic modelling of the electrical behaviour of a commercial
849 advanced alkaline water electrolyser. Int J Hydrogen Energy 2012;37:18598–614.
850 doi:10.1016/j.ijhydene.2012.09.125.
851 [60] Matzen M, Alhajji M. Chemical storage of wind energy by renewable methanol production :
852 Feasibility analysis using a multi-criteria decision matrix 2015;93.
853 doi:10.1016/j.energy.2015.09.043.
854 [61] Ulleberg Ø. Stand-Alone Power Systems for the Future: Optimal Design, Operation &
855 Control of Solar-Hydrogen Energy Systems. Norwegian University of Science and
856 Technology Trondheim, 1998.
857 [62] Van-Dal ÉS, Bouallou C. Design and simulation of a methanol production plant from CO2
858 hydrogenation. J Clean Prod 2013;57:38–45. doi:10.1016/j.jclepro.2013.06.008.
859 [63] Al-Malah KIM. Aspen Plus®. Hoboken, NJ, USA: John Wiley & Sons, Inc.; 2016.
860 doi:10.1002/9781119293644.
861 [64] Ni M, Leung MKH, Leung DYC. Parametric study of solid oxide fuel cell performance.
862 Energy Convers Manag 2007;48:1525–35. doi:10.1016/j.enconman.2006.11.016.
863 [65] Sengodan S, Lan R, Humphreys J, Du D, Xu W, Wang H. Advances in reforming and partial
864 oxidation of hydrocarbons for hydrogen production and fuel cell applications. Renew Sustain
865 Energy Rev 2018;82:761–80. doi:10.1016/j.rser.2017.09.071.
866 [66] Doherty W, Reynolds A, Kennedy D. Computer simulation of a biomass gasification-solid
867 oxide fuel cell power system using Aspen Plus. Energy 2010;35:4545–55.
868 doi:10.1016/j.energy.2010.04.051.
869 [67] Macchi E, Astolfi M, editors. Organic Rankine Cycle (ORC) Power Systems. Elsevier; 2017.
870 doi:10.1016/C2014-0-04239-6.
871 [68] Drescher U, Brüggemann D. Fluid selection for the Organic Rankine Cycle (ORC) in
872 biomass power and heat plants. Appl Therm Eng 2007;27:223–8.
873 doi:10.1016/j.applthermaleng.2006.04.024.
874 [69] Victor RA, Kim JK, Smith R. Composition optimisation of working fluids for organic Rankine
875 cycles and Kalina cycles. Energy 2013;55:114–26. doi:10.1016/j.energy.2013.03.069.
876 [70] Linstrom P. NIST Chemistry WebBook, NIST Standard Reference Database 69. Natl Inst
877 Stand Technol 1997. doi:https://doi.org/10.18434/T4D303.
878 [71] Benzene | C6H6 - PubChem n.d. https://pubchem.ncbi.nlm.nih.gov/compound/Benzene
879 (accessed March 2, 2020).
880 [72] Ni M, Leung MKH, Leung DYC. Parametric study of solid oxide steam electrolyzer for
881 hydrogen production. Int J Hydrogen Energy 2007;32:2305–13.
882 doi:10.1016/j.ijhydene.2007.03.001.
883 [73] Buonomano A, Calise F, Dentice M, Palombo A, Vicidomini M. Hybrid solid oxide fuel cells –
884 gas turbine systems for combined heat and power : A review. Appl Energy 2015;156:32–85.
885 doi:10.1016/j.apenergy.2015.06.027.
886 [74] Wendel CH, Kazempoor P, Braun RJ. Novel electrical energy storage system based on

reversible solid oxide cells: System design and operating conditions. J Power Sources 2015;276:133–44. doi:10.1016/j.jpowsour.2014.10.205.
[75] Barelli L, Bidini G, Cinti G. Airflow Management in Solid Oxide Electrolyzer (SOE) Operation: Performance Analysis. ChemEngineering 2017;1:13. doi:10.3390/chemengineering1020013.
[76] Cascetta M, Cau G, Puddu P, Serra F. Experimental investigation of a packed bed thermal energy storage system. J Phys Conf Ser 2015;012018. doi:10.1088/1742-6596/655/1/012018.
[77] Cascetta M, Serra F, Arena S, Casti E, Cau G, Puddu P. Experimental and Numerical Research Activity on a Packed Bed TES System. Energies 2016;9:1–13. doi:10.3390/en9090758.
[78] Vasiliev LL, Burak VS, Kulakov AG, Mishkinis DA, Bohan P V. Heat storage for a bus petrol internal-combustion engine. In: Hutter K, Wang Y, Beer H, editors. Adv. Cold-Region Therm. Eng. Sci., Berlin, Heidelberg: Springer Berlin Heidelberg; 1999, p. 585–94.
[79] Weber R, Dorer V. Long-term heat storage with NaOH. Vacuum 2008;82:708–16. doi:10.1016/j.vacuum.2007.10.018.
[80] Porisini FC. Salt hydrates used for latent heat storage: Corrosion of metals and reliability of thermal performance. Sol Energy 1988;41:193–7. doi:10.1016/0038-092X(88)90136-3.
[81] Agyenim F, Hewitt N, Eames P, Smyth M. A review of materials, heat transfer and phase change problem formulation for latent heat thermal energy storage systems (LHTESS). Renew Sustain Energy Rev 2010;14:615–28. doi:10.1016/j.rser.2009.10.015.
[82] Lonis F, Tola V, Cascetta M, Arena S, Cau G. Performance evaluation of an integrated energy system for the production and use of renewable methanol via water electrolysis and CO2 hydrogenation 2019;020099. doi:10.1063/1.5138832.
[83] Héder M. From NASA to EU: The evolution of the TRL scale in Public Sector Innovation. Innov J 2017;22:1–23.
[84] FLEXCHX. Review of electrolysis technologies and their integration alternatives - FLEXCHX Flexible combined production of power, heat and transport fuels from renewable energy sources 2018:35.
[85] Pérez-Fortes M, Tzimas E. Techno-economic and environmental evaluation of CO2 utilisation for fuel production. Synthesis of methanol and formic acid. 2016. doi:10.2790/981669.
[86] Pérez-Fortes M, Schöneberger JC, Boulamanti A, Tzimas E. Methanol synthesis using captured CO2 as raw material : Techno-economic and environmental assessment. Appl Energy 2016;161:718–32. doi:10.1016/j.apenergy.2015.07.067.